Organic & Biomolecular Chemistry

PAPER

View Article Online
View Journal

Cite this: DOI: 10.1039/c8ob02255k

Methyl 5-MeO-*N*-aminoanthranilate, a minimalist fluorogenic probe for sensing cellular aldehydic load†

Mojmír Suchý,[a,c] Caitlin Lazurko,[a] Alexia Kirby,[b,c] Trina Dang,[a] George Liu[a] and Adam J. Shuhendler *[a,c]

Methyl 5-MeO-*N*-aminoanthranilate, a fluorogenic probe comprising a single substituted benzene ring has been applied towards the fluorescence detection of endogenous carbonyls through rapid, catalyst-free complexation of these bio-derived markers of cell stress under physiological conditions. The products formed during the reaction between the probe and aldehydic products of lipid peroxidation, including malondialdehyde and long-chain aliphatic aldehydes relevant to the oxidative decomposition of cell membranes, have been evaluated. Live cell imaging of diethyl maleate-induced oxidative stress with or without pretreatment with α-tocopherol was carried out, with the result suggesting that the presented molecule might serve as a minimalist molecular probe capable of cellular "Aldehydic Load" detection by fluorescence microscopy. This work also outlines functional constraints of the fluorogenic probe (*i.e.* intramolecular cyclization), providing a realistic evaluation of methyl 5-MeO-*N*-aminoanthranilate for fluorescence-based aldehyde detection.

Received 12th September 2018,
Accepted 1st November 2018

DOI: 10.1039/c8ob02255k

rsc.li/obc

Introduction

Anthranilic acid (**1a**, Fig. 1) and methyl anthranilate (**1b**, Fig. 1) are among the simplest naturally occurring fluorophores, exhibiting long excited state life times (8.7 ns) along with high quantum yields in aqueous solution (Φ ~0.60).[1] Although these properties appear to make the anthranilic acid-based fluorophores attractive probes for molecular biology, their use in the context of the development of imaging probes is still in its infancy.[2] This can be in part attributed to the fact that anthranilic acid-based fluorophores require high energy excitation (320–350 nm) and emit in the violet to blue region (λ_{em} 410–470 nm).[1] Moreover, the synthetic methodologies describing their incorporation into larger molecular entities are rather limited.[3]

Kool and co-workers have recently shown that substituted anthranilic acids can auto-catalyze the reaction between hydrazines and carbonyl compounds (aldehydes and ketones denoted herein as carbonyls) to form hydrazones.[4] When anthranilic acid is converted into the corresponding hydrazine (*N*-aminoanthranilic acid, **1c**, Fig. 1), the rate of the reaction with carbonyls increases dramatically even surpassing that associated with strain-promoted "click" reactions, which makes *N*-aminoanthranilates attractive reactive head-groups for the rapid, catalyst-free trapping of biogenic carbonyls under physiological conditions.[5]

It is now well established that the exposure of humans to carbonyls has a negative impact on health and well-being.[6]

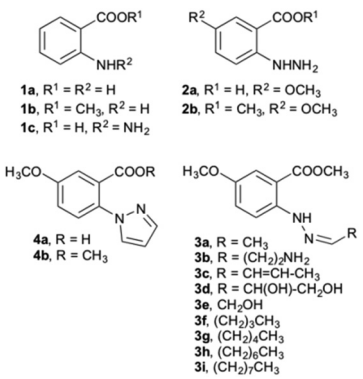

Fig. 1 Structures of anthranilic acids and anthranilates **1a–1c**, **2a**, **2b**, hydrazones **3a–3i**, pyrazoles **4a** and **4b**.

[a]*Department of Chemistry & Biomolecular Scences, University of Ottawa, Ottawa, ON, Canada. E-mail: ashuhend@uottawa.ca*
[b]*Department of Biology, University of Ottawa, Ottawa, ON, Canada*
[c]*University of Ottawa Heart Institute, Ottawa, ON, Canada*

† Electronic supplementary information (ESI) available: Full spectral characterization of hydrazones **3f–3i**, fluorescence spectra associated with pyrazoles **4a** and **4b**, full view of the ^{1}H NMR spectra associated with the detailed kinetic analysis. See DOI: 10.1039/c8ob02255k

Although some carbonyls are present in the environment as a consequence of industrial operations (*e.g.* acetone, formaldehyde), many simple carbonyls (*e.g.* acetaldehyde, glyceraldehyde, pyruvate) are also produced endogenously *via* tightly regulated metabolic pathways.[6] Increased production of carbonyls upon the disruption of homeostasis often times underlies early stages of various pathologies, including diabetes (*e.g.* acetone),[7] cancer (*e.g.* simple aliphatic aldehydes)[8] cardiovascular diseases [*e.g.* acrolein, malondialdehyde (MDA)][9] or traumatic brain injury (*e.g.* 3-aminopropanal).[10] The ability to properly design, synthesize and evaluate molecular probes capable of *in vitro* or *in vivo* mapping of total endogenous carbonyls (denoted herein as Aldehydic Load) is of significant interest to the scientific community,[11] as the outcomes of these research efforts are expected to facilitate our fundamental understanding of, and ability to diagnose, a wide range of illnesses affecting a significant part of the global population.

The development of molecular imaging probes capable of reporting on Aldehydic Load at both the *in vitro* and *in vivo* scales is one of the key research avenues currently pursued in our laboratory. We have recently shown that 5-MeO-*N*-aminoanthranilic acid (**2a**, Fig. 1), a simple anthranilic acid-based hydrazine can act as a Chemical Exchange Saturation Transfer Magnetic Resonance Imaging (CEST MRI) contrast agent upon reaction with endogenous aldehydes (*e.g.* acetaldehyde, 3-aminopropanal).[5b] During the course of our studies, we have also prepared methyl 5-MeO-*N*-aminoanthranilate (**2b**, Fig. 1) and allowed it to react with several endogenous carbonyls. The majority of the products we obtained upon reaction with aldehydes (hydrazones **3a–3e**, Fig. 1) were found to fluoresce in the blue to blue-green region of the spectrum; therefore we decided to study their fluorescence in greater detail. As described recently, we have acquired excitation–emission matrices (EEM) associated with compounds **3a–3e** (Fig. 1), and have concurrently developed a novel pattern matching algorithm for the fluorescent fingerprinting of biogenic carbonyls.[12] This approach allowed us to determine both the total amount of aldehyde (*i.e.* Aldehydic Load), as well as the identity of individual components of carbonyl mixtures. As an expansion to our previous studies, we are describing herein the fluorescence properties associated with hydrazones derived from longer chain aliphatic aldehydes as putative end-products of lipid peroxidation (compounds **3f–3i**, Fig. 1), and validating the use of **2b** as a fluorogenic probe capable of mapping Aldehydic Load *via* live cell microscopy in a model of oxidative stress. We have also carried out detailed mechanistic studies to elucidate the mechanism of the reaction between methyl 5-MeO-*N*-aminoanthranilate (**2b**, Fig. 1) and the dialdehyde MDA to form a pyrazole ring through an *in situ* detected hydrazone intermediate. The further understanding of the reaction mechanisms of methyl 5-MeO-*N*-aminoanthranilate with biogenic carbonyls reported in this work supports the utility of this minimalist fluorogenic probe, and advocates for its value as a novel tool for studying the chemical biology of lipid peroxidation in live cells.

Results and discussion

Preparation of hydrazone/pyrazole standards and evaluation of their fluorescence properties

Chemical synthesis of the probes was carried out as outlined in Scheme 1. Reaction of methyl 5-MeO-*N*-aminoanthranilate (**2b**) with simple longer chain aliphatic aldehydes (pentanal, hexanal, octanal, nonanal) afforded hydrazones **3f–3i** in good yields (61–83%). The final compounds were purified by flash column chromatography (FCC) and were obtained as inseparable mixtures of *E* and *Z* isomers in approximately a 2 : 3 ratio (major isomer not identified). Observed results are in contrast with the synthesis of previously described hydrazones (**3a–3e**, Fig. 1),[12] which were obtained either as a single isomer, or where the amount of the minor isomer was negligible (<5%). Fluorescence spectra of hydrazones **3f–3i** were acquired in phosphate buffered saline (1× PBS, pH 7.2) containing up to 10% DMSO (Fig. 2), and relative quantum yields (Φ) were determined using harmane as standard (Table 1).[13]

While the excitation wavelengths appear to be independent of the hydrazone structure and only vary by 6 nm, the emission wavelengths as well as Stoke's shifts decrease slightly with increasing length of the carbon chain. Fluorescence quantum yields were found to be relatively low, possibly a consequence of the presence of two inseparable isomers, and decreased with an increased length of aldehyde carbon chain. When 5-MeO-*N*-aminoanthranilic acid (**2a**) or methyl 5-MeO-*N*-aminoanthranilate (**2b**) were treated with MDA tetramethyl acetal, pyrazoles **4a** and **4b** were obtained in moderate yield (Scheme 1) upon purification by FCC as described recently.[12]

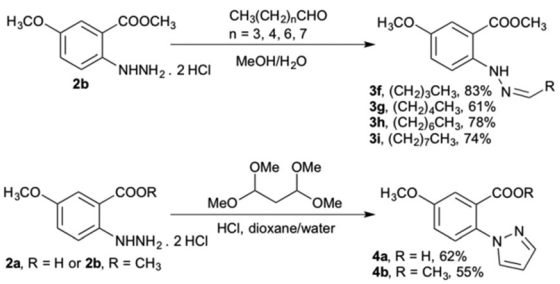

Scheme 1 Preparation of hydrazones **3f–3i** and pyrazoles **4a** and **4b**.

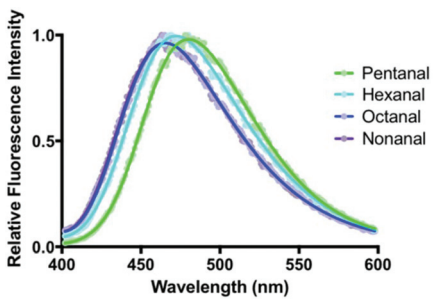

Fig. 2 Emission scans for hydrazones derived from **2b** and aliphatic aldehydes **3f** (green), **3g** (cyan), **3h** (blue), and **3i** (purple) acquired with λ_{ex} = 370 nm.

Table 1 Fluorescence properties associated with hydrazones **3f–3i**

Compound	ϕ (harmane)	λ_{ex} (nm)	ε (m^2 mol^{-1})	λ_{em} (nm)	Stoke's shift (nm)
3f	0.17	372	5631	480	108
3g	0.08	376	7107	475	99
3h	0.08	377	8410	467	90
3i	0.06	378	8025	466	88

Pyrazole formation from MDA and methyl 5-MeO-*N*-aminoanthranilate (2b) proceeds through a long-lived fluorescent hydrazone intermediate

Malondialdehyde (MDA, **5**, Scheme 2), a terminal product of polyunsaturated fatty acid peroxidation mediated by reactive oxygen species (ROS) is regarded as a classical marker of oxidative stress.[14] MDA occurs as an equilibrium of two tautomers (Scheme 2), is a known mutagen,[15] and has been associated with early stages of various pathologies (*e.g.* cancer,[16] atherosclerosis,[17] stroke,[18] Alzheimer's disease[19]). MDA has classically been assayed in cells or tissue extracts through treatment with thiobarbituric acid (**6**, Scheme 2) with the formation of a red coloured dye **7** under harsh conditions.[20]

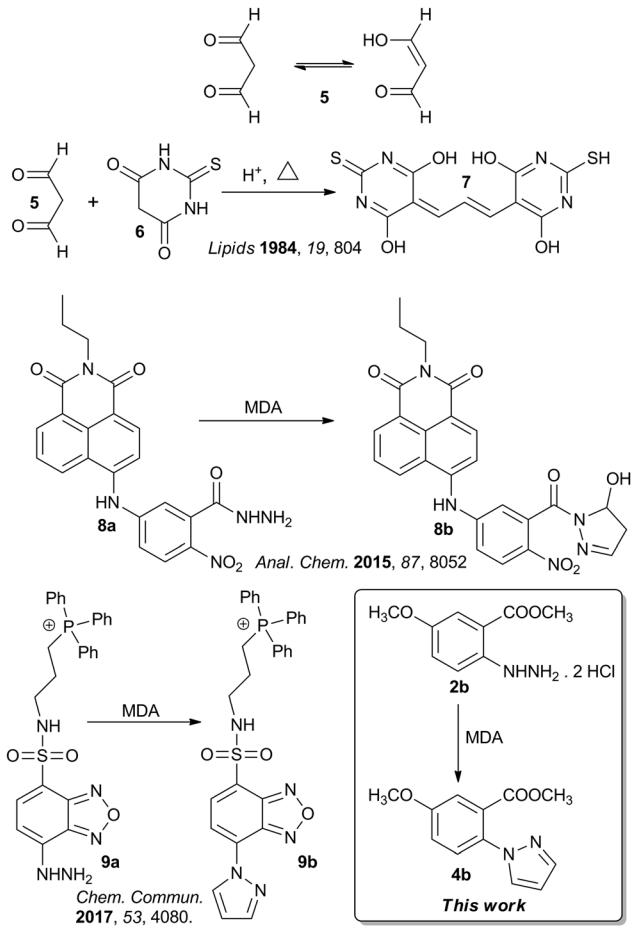

Scheme 2 Structure of MDA, colourimetric (**6** → **7**) and fluorogenic probes (**8a** → **8b**; **9a** → **9b**) used for its detection previously. The fluorogenic probe (**2b** → **4b**) investigated in this work is structurally simpler than previous probe examples.

The development of a molecular imaging probe capable of *in situ* complexation of MDA in live cells in order to more accurately map concentrations has been challenging due to the high reactivity of MDA in living systems, which is partly attributable to its presence in two tautomeric forms.[21] Recent efforts toward this end include two green fluorescent probes (**8a**,[22] **9a**,[23] Scheme 2), bearing a hydrazide/hydrazine subunit reported to quench fluorescence *via* photoinduced electron transfer (PET). Upon reaction with MDA, a five-membered pyrazolidine/pyrazole ring is formed (compounds **8b**, **9b**, Scheme 2), limiting PET to result in a strong fluorescence turn-on.[22,23] Both **8a** and **9a** show excellent selectivity toward MDA, as no fluorescence response is observed upon exposure to other carbonyls.[22,23] Interestingly, this observation is in contrast with our results using methyl 5-MeO-*N*-aminoanthranilate (**2b**), wherein the reaction with a range of simple endogenous carbonyls leads to the formation of fluorescent hydrazones (*e.g.* compounds **3a–3i**).[12] Although the detailed mechanism of the fluorescence signal turn on associated with the **8a** → **8b** transformation has been proposed based on NOESY measurements,[22] no evidence for the suggested mechanism associated with the signal turn on upon **9a** → **9b** conversion has been provided.[23] Due to differential aldehyde selectivity of **2b** relative to **8a** and **9a**, a detailed mechanistic evaluation of the reaction of MDA with 5-MeO-*N*-aminoanthranilic acid (**2a**) and methyl 5-MeO-*N*-aminoanthranilate (**2b**) was undertaken.

Compound **2b** (Fig. 1, Scheme 2) contains a hydrazine subunit and is known to form a pyrazole ring (compound **4b**, Scheme 2) upon exposure to MDA.[12] The structure of pyrazole **4b** is simple, with well-resolved resonances in its ^{1}H NMR spectrum,[12] which permitted a detailed ^{1}H NMR-based kinetic analysis to be carried out in order to fully understand the transformation of 5-MeO-*N*-aminoanthranilic acid (**2a**) and methyl 5-MeO-*N*-aminoanthranilate (**2b**) to pyrazoles **4a** and **4b** upon reaction with MDA.

Since the main chemical shift differences due to pyrazole formation were expected in the aromatic region (6–8 ppm), only changes occurring within this range are depicted in Fig. 3 and discussed below. Note that full views of the spectra can be found in Supporting Fig. S1 and S2.† Briefly, within this region both hydrazines **2a** and **2b** exhibit three distinct signals (**2a**, d, 7.26 ppm, J = 3 Hz, H^6; d, 7.08 ppm, J = 9 Hz, H^3; dd, 7.01 ppm, J = 9, 3 Hz, H^4; **2b**, d, 7.52 ppm, J = 3 Hz, H^6; dd, 7.20 ppm, J = 9, 3 Hz, H^4; d, 7.05 ppm, J = 9 Hz, H^3) fully consistent with the substitution pattern present in **2a** and **2b**.

Baseline ^{1}H-NMR spectra were acquired of separate solutions of 1 mg of **2a** or **2b** in 1× PBS, pH 7.2 containing 10% DMSO-D_6, followed by the addition of 1 drop of a 1 M solution of MDA tetramethyl acetal in 1 M HCl, known to form MDA *in situ*.[24] Further acquisitions of ^{1}H NMR spectra occurred immediately (1 min), 2 min, 4 min, 20 min and, for compound **2b** only, 2 h after MDA addition (Fig. 3). To allow for this rapid spectral acquisition following addition of MDA, neither locking of the signal nor shimming was carried out. The reaction of hydrazines **2a** and **2b** with MDA led to the rapid formation (within 1 min) of new peaks associated with a putative

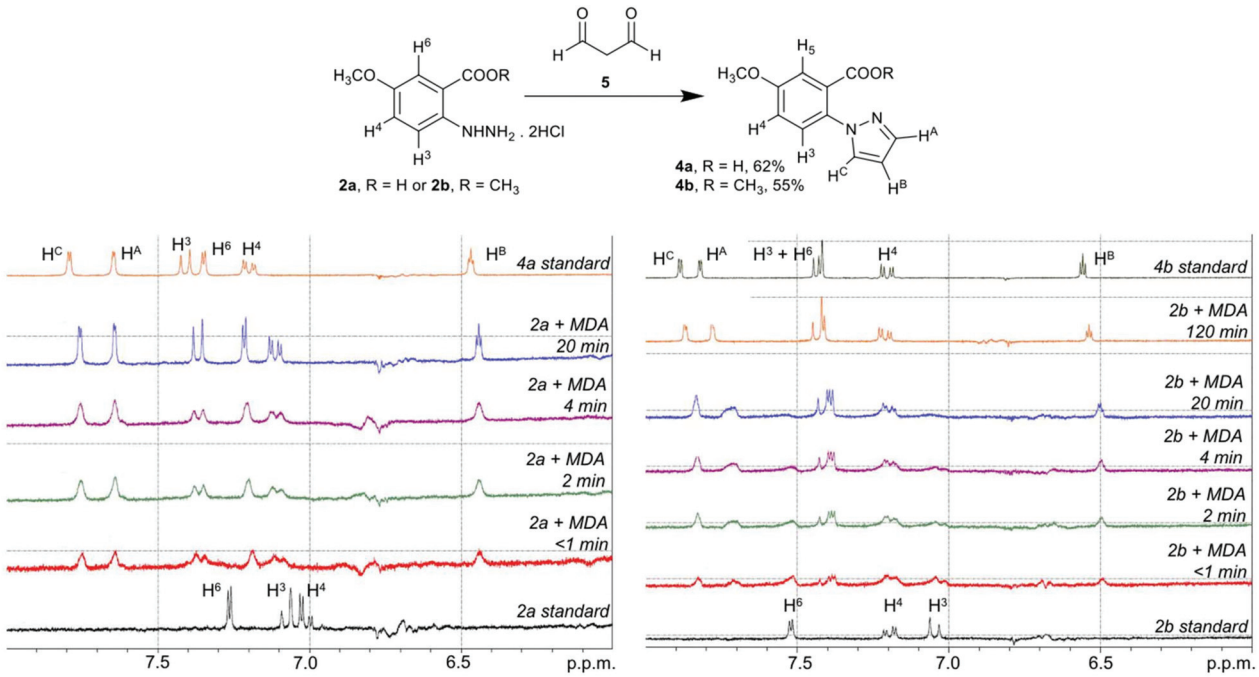

Fig. 3 Detailed ^{1}H NMR analysis of the reactions between 5-MeO-*N*-aminoanthranilic acid (**2a**) and MDA (left), or methyl 5-MeO-*N*-aminoanthranilate (**2b**) and MDA (right). Spectra shown are before MDA addition (black), and <1 min (red), 2 min (green), 4 min (purple), 20 min (blue), and 2 h (orange) after MDA addition. Brown and grey spectra are those of authentic standards **4a** (left) or **4b** (right).

pyrazole ring, as well as a slight change in benzene ring chemical shifts associated with starting materials **2a** and **2b**. Three new signals at *ca.* 7.8 (H^C), 7.7 (H^A) and 6.5 ppm (H^B) are observed in both instances and their intensity increases with time (Fig. 3). The presence of the new signals is fully consistent with the formation of the pyrazole scaffold in both, **4a** and **4b** (see the Experimental and ESI† for the details), with only slight changes in chemical shifts (≤0.1 ppm) between the products of the reactions observed at the terminal time points (**4a**, 20 min; **4b**, 2 h) and corresponding pyrazole standards **4a** and **4b** having their spectra acquired under identical conditions.

This deviation in chemical shift is likely caused by the fact that the spectrometer was not shimmed prior to the acquisition of spectra during the time-course study. Consistent with our previous observations,[5b] the reaction of hydrazine **2a** with MDA occurred very rapidly and only traces of the hydrazone intermediate can be observed as a small shoulder associated with the signal at *ca.* 7.7 ppm (H^A) in the NMR spectra acquired at earlier time points up until 4 min (Fig. 3, left). However, the signal observed at 7.7 ppm (H^A) was of particular interest in the NMR spectra associated with hydrazine **2b** wherein the signal is broad and unresolved even after 20 min of reaction, and a distinct doublet is observed after 2 h (Fig. 3, right). This observation prompted us to propose that a short-lived hydrazone intermediate is present in solution and observable by NMR spectroscopy.

In order to further investigate the formation and fate of the proposed hydrazone intermediate observed by ^{1}H NMR spectroscopy, we performed an identical experiment to that performed for the NMR study however using fluorescence spectroscopy as read out. Fluorescence spectra associated with pyrazoles **4a** and **4b** were measured in 1× PBS, pH 7.2, containing 10% DMSO (Fig. ESI48 and 49†). Pyrazole **4a** is a weak (Φ < 0.02, harmane) blue fluorophore (λ_{ex} 258 nm, λ_{em} 391 nm, Stoke's shift 133 nm), which precluded a detailed investigation of the reaction of **2a** with MDA by fluorescence spectroscopy. However, the replacement of the carboxylic acid moiety in pyrazole **4b** with the ester leads to a significant increase (>20 fold) in quantum yield (Φ 0.45, harmane)[12] as well as a red shift of both excitation and emission wavelengths (**4b**, λ_{ex} 307 nm, λ_{em} 410 nm, Stoke's shift 103 nm), allowing for a detailed fluorescence-guided investigation of the reaction between methyl 5-MeO-*N*-aminoanthranilate (**2b**) and MDA.

Upon mixing hydrazine **2b** with MDA under illumination by UV lamp (λ_{ex} 365 nm), the evolution of blue-green fluorescence was observed within 1 minute (Fig. 4a), which was red-shifted relative to the expected fluorescence of the synthesized pyrazole standard, compound **4b** (λ_{em} 410 nm). Detailed measurement of the fluorescence associated with the obtained mixture revealed two fluorescent species in solution: one with spectral properties expected from compound **4b** (λ_{ex} 307 nm, λ_{em} 410 nm), and the other with λ_{ex} 371 nm as an optimal excitation wavelength and associated emission at λ_{em}478 nm (Stoke's shift 107 nm, Fig. 4b). When the mixture was left at room temperature (rt) for 30 minutes, the initially observed blue-green fluorescence was no longer visible, but instead the mixture produced a deep blue fluorescence with photophysical properties matching those of **4b**. Fluorescence kinetic measurements were carried out that recapitulated these qualitative observations

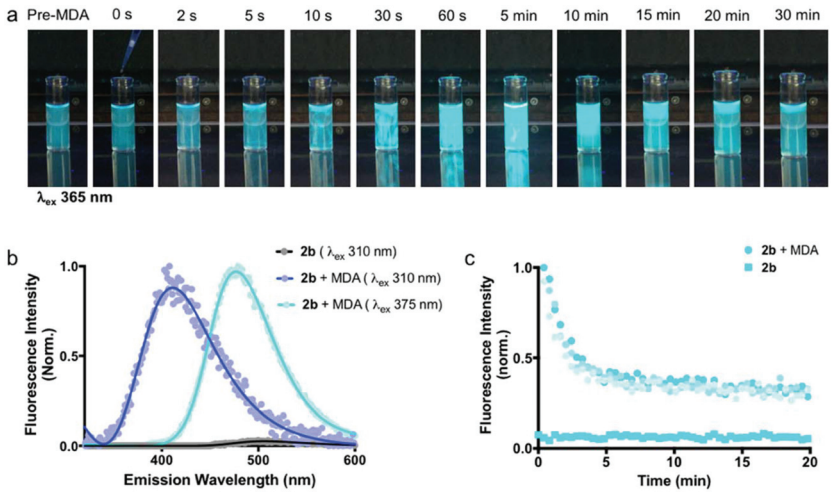

Fig. 4 Methyl 5-MeO-*N*-aminoanthranilate (**2b**) as a fluorogenic probe for the detection of MDA. (a) MDA was added to a 25 μM PBS solution of **2b** (pH 7.2) under illumination at 365 nm, and photographed at indicated time points. (b) Emission spectra of 1 μM **2b** (black), or **2b** after 1 min incubation with 5 eq. MDA at 37 °C and excited at 310 nm (blue) or 375 nm (cyan). (c) Formation and rapid decay of short lived intermediate **10** formed in the reaction between methyl 5-MeO-*N*-aminoanthranilate (**2b**) and MDA followed by fluorescence spectroscopy with $\lambda_{ex}/\lambda_{em}$ = 375/480 nm. Kinetics of 25 μM **2b** alone (squares) and **2b** + MDA (circles) are shown, with three individual trials of **2b** + MDA shown (light, medium, and dark cyan).

(Fig. 4c). An initial formation of the blue-green fluorescent species takes place rapidly, followed by a rapid decrease of the fluorescent signal at λ_{em} 480 nm by 50% within 5 minutes, and then a slower decrease over a longer period of time.

Considering the results of the fluorescence-based kinetic study along with those from the detailed NMR experiment, a mechanism for the reaction of **2b** with MDA is proposed (Scheme 3). While we believe that an identical mechanism operates in the case of the transformation **2a** → **4a** supported by the NMR study, we were unable to support this hypothesis by fluorescence measurements. The reaction of **2b** with MDA leads to the formation of the hydrazone intermediate **10**, which is transiently stabilized by the presence of a hydrogen bond between the terminal hydrazone nitrogen and the hydroxyl group of the enol tautomer of intermediate **10**. The enol tautomer would be favoured by the intramolecular hydrogen bond resulting in a pseudo-aromatic six-membered ring. The nucleophilic attack of the ring-proximal nitrogen group present in the hydrazone moiety onto the electrophilic carbonyl would then take place, ultimately leading to the formation of pyrazole **4b** (Scheme 3). Importantly, the intensity of the observed blue-green emission peak was dependent on MDA concentration, supporting the hypothesis that the observed fluorescence was associated with a semi-stable reaction intermediate **10** (Fig. 5).

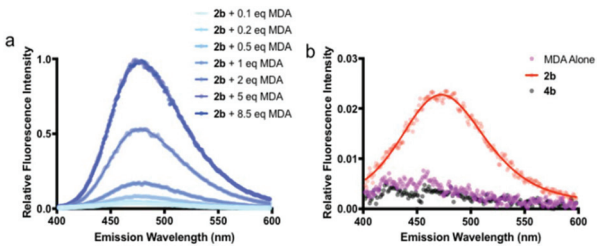

Fig. 5 The formation of the fluorescent hydrazone intermediate **10** is dependent upon MDA concentration. (a) A 1 μM solution of **2b** in PBS (pH 7.2) was mixed with the indicated molar equivalents of MDA and an emission scan was recorded immediately after mixing using λ_{ex} 375 nm (blue curves). (b) Emission scans for MDA alone (open circles), **2b** alone (red), and the pyrazole standard **4b** (black) are also shown. Note the difference in the y-axis scaling between panels a and b.

Cyclization of methyl 5-MeO-*N*-aminoanthranilate (2b) in PBS buffer

During our initial experiments involving solutions of methyl 5-MeO-*N*-aminoanthranilate dihydrochloride (**2b**) in PBS, we noted the evolution of deep-blue fluorescence over 5 min from an initially non-fluorescent probe stock solution. To understand this phenomenon, we evaluated the stability of hydrazine **2b** in PBS at 37 °C (Fig. 6). A significant (~10 fold) fluorescence signal increase (λ_{em} 421 nm) was observed within

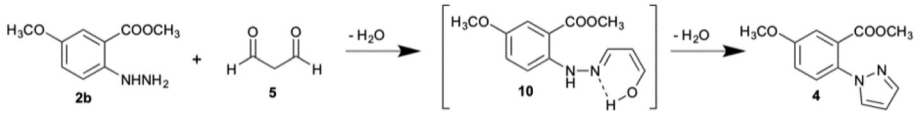

Scheme 3 Reaction between hydrazine **2b** and MDA proceeds *via* short lived intermediate **10**.

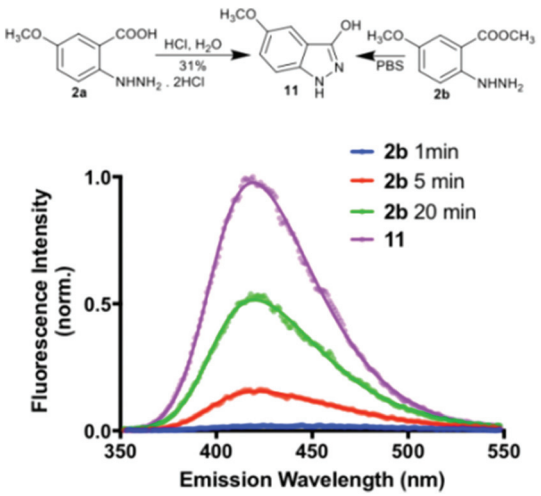

Fig. 6 Cyclization of methyl 5-MeO-*N*-aminoanthranilate (**2b**) in PBS solution. Probe **2b** was incubated at 37 °C in PBS (pH 7.2) for 1 (blue), 5 (red), and 20 min (green), and an emission scan was recorded with λ_{ex} 310 nm. The emission spectrum of the standard indazole **11** is shown for comparison.

5 minutes of incubation, which continued to increase over time. It is known that heating *N*-aminoanthranilic acids (*e.g.* **2a**) in concentrated HCl results in the formation of indazoles.[25] This reaction involves a strong mineral acid-catalyzed intramolecular nucleophilic attack of the terminal hydrazine nitrogen onto the carbonyl group with the formation of a tetrahedral intermediate, followed by its collapse and subsequent aromatization to afford blue fluorescent indazoles. Our hypothesis (Fig. 6) was that a similar reaction was taking place when hydrazine **2b** is dissolved in PBS buffer. Although the solution of **2b** is neutral (pH ~7.2), the concentration of **2b** is low enough (10^{-6} M) to favour intramolecular reactions. Importantly, the ester moiety makes the carbonyl group in **2b** more prone to intramolecular nucleophilic attack by the terminal hydrazine nitrogen since methanol is a relatively better leaving group, facilitating the collapse of the tetrahedral intermediate. We have prepared indazole **11** (in 31% yield, Fig. 6) by heating 5-MeO-*N*-aminoanthranilic acid (**2a**) according to a previous method,[25] and compared the fluorescence emission spectra (λ_{em} 421 nm) of **11** to those obtained by simple incubation of **2b** in PBS. As shown in Fig. 6, a good match in emission maxima between standard **11** and stock solution containing **2b** was observed upon excitation at 310 nm. Excitation at higher wavelengths (λ_{ex} 375 nm) required to induce hydrazone fluorescence, resulted in background levels of fluorescence emission from the indazole (Fig. ESI50a†). Furthermore, the *pseudo*-first order rate constant for the cyclization reaction in PBS (k_{obs} = 0.009 ± 0.002 min^{-1}) was 10-fold lower than that for hydrazone formation with hexanal as a test aldehyde (k_{obs} = 0.100 ± 0.002 min^{-1}) as determined by previously published methods (Fig. ESI50b†).[5] Together, this suggests that indazole formation, while limiting levels of **2b** in PBS, would not result in artifactual fluorescence emission upon aldehyde sensing with compound **2b**. Importantly, the spontaneous cyclization of **2b** can be significantly limited by preparation of stock solutions in DMSO and guarding them from light, where cyclization to **11** was found to be slow (<5% conversion after 24 h) as indicated by ^{1}H NMR inspection.

Specificity of fluorogenic response of hydrazone 2b to biogenic carbonyls, metabolites, and ions

In addition to MDA, we assayed the fluorogenic response of hydrazine **2b** towards endogenous carbonyl compounds, including aliphatic aldehydes (formaldehyde, acetaldehyde, pentanal, hexanal, octanal, nonanal), more complex aldehyde metabolites (glyoxal, methylglyoxal, crotonaldehyde, glyceraldehyde), cofactors (pyridoxal phosphate), ketones (acetone, pyruvate, butanedione, acetylacetone), glutathione, and biogenic cations (Ca^{2+}, Cu^{2+}, Fe^{3+}, Mg^{2+}, Mn^{2+}, Zn^{2+}, Fig. 7). Among the carbonyls examined, hydrazine **2b** showed limited fluorescence signal turn-on in the presence of ketones, glutathione and some complex aldehydes (crotonaldehyde, glyoxal, pyridoxalphosphate). While some biogenic metal cations (Ca^{2+}, Fe^{3+}, Mg^{2+}) appeared to produce negligible fluorescence in the presence of **2b**, a moderate fluorescence signal turn-on is observed from Cu^{2+}, Mn^{2+} and Zn^{2+} (Fig. 7). This weak fluorescence response is possibly attributable to the suitability of both the hydrazino- and methyloxycarbonyl groups as ligands for Cu^{2+}, Mn^{2+} and Zn^{2+}, possibly promoting the formation of metal complexes in solution. In addition to glyceraldehyde and methylglyoxal, simple aliphatic aldehydes (formaldehyde, acetaldehyde, pentanal, hexanal, octanal, and nonanal) showed a substantial fluorescence signal turn-on upon reaction with hydrazine **2b** (Fig. 7).

From a diagnostic standpoint, increased concentrations of pentanal, hexanal, octanal and nonanal were found in the exhaled breath of lung cancer patients when compared to healthy smoker and non-smoker volunteers.[8] While the formation of hexanal results from the oxidative cleavage of linoleic or arachidonic acid[26] and hexanal is considered a general marker of oxidative stress,[27] other aldehydes might also result from lipid peroxidation if specific unsaturated fatty acids are present in tumour cell membranes. Derivatization of these ali-

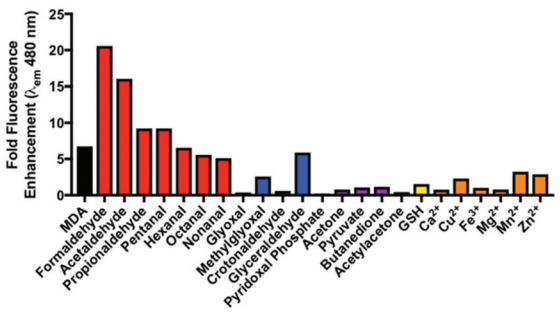

Fig. 7 Methyl 5-MeO-*N*-aminoanthranilate (**2b**) shows broad specificity to aliphatic aldehydes. The fold fluorescence enhancement relative to **2b** alone was recorded with $\lambda_{ex}/\lambda_{em}$ 375/480 nm following 1 min of incubation of 1 μM solutions of **2b** in PBS (pH 7.2) with 5 eq. of MDA (black bar), simple aliphatic aldehydes (red bars), dialdehydes and more complex aldehydes (blue bars), ketones (purple bars), glutathione (yellow bar) and biogenic metal cations (orange bars).

phatic aldehydes as biomarkers of lung cancer and analysis by fluorescent methods may present an alternative to tandem gas chromatography mass spectrometry (GC-MS) analysis currently used.[8,28] Compared to GC-MS analysis requiring expensive instrumentation, as well as sample processing leading to potential inaccuracies, fluorescence assays are significantly easier to perform and may be better suited to the point-of-care determination of longer chain aliphatic aldehydes. Future studies will seek to apply fluorescence-based aldehyde fingerprinting that uses **2b** as derivatizing agent for the identification of hydrazones **3f–3i** in complex mixtures to rapidly determine their identities with a low-cost technique.[12] Overall our results indicate that hydrazine **2b** could serve as a fluorogenic probe for Aldehydic Load, providing for the detection of a range of aliphatic aldehydes and MDA, which comprise catabolic products of lipid peroxidation.

Imaging Aldehydic Load changes due to lipid peroxidation by live cell microscopy

While there are a variety of biochemical processes that can result in the production of aldehydes in cells and tissues, the major source of aliphatic aldehydes is the decomposition of the cell membrane due to lipid peroxidation.[14] Since the fluorogenic response of **2b** to aldehydes spans a broad range of potential products of lipid peroxidation to yield fluorescent hydrazones with spectral properties amenable to conventional fluorescence microscopy (*i.e.* λ_{ex} 370 nm, λ_{em} 480 nm), we sought to apply this probe to live cell imaging. A well-characterized model of lipid peroxidation was implemented, comprising human HEK293 cells treated with diethyl maleate (DEM), which perturbs cellular redox status with the endpoint of cell membrane catabolism through oxidative lipid degradation, and/or with α-tocopherol (α-TOH), nature's most effective antioxidant previously shown to limit DEM-induced lipid peroxidation.[29] Cells were either left untreated (Fig. 8b, g and l), or were treated with 1.5 mM DEM for 1 h (Fig. 8c, h and m) or 2 h (Fig. 8d, i and n) in order to induce lipid peroxidation prior to incubation with **2b** for 5 min. Micrographs show limited fluorescence in untreated HEK293 cells, which is expected due to a homeostatic flux of metabolic aldehydes and carbonyls such as glyceraldehyde and pyruvate. However, a substantial fluorescence enhancement is observed

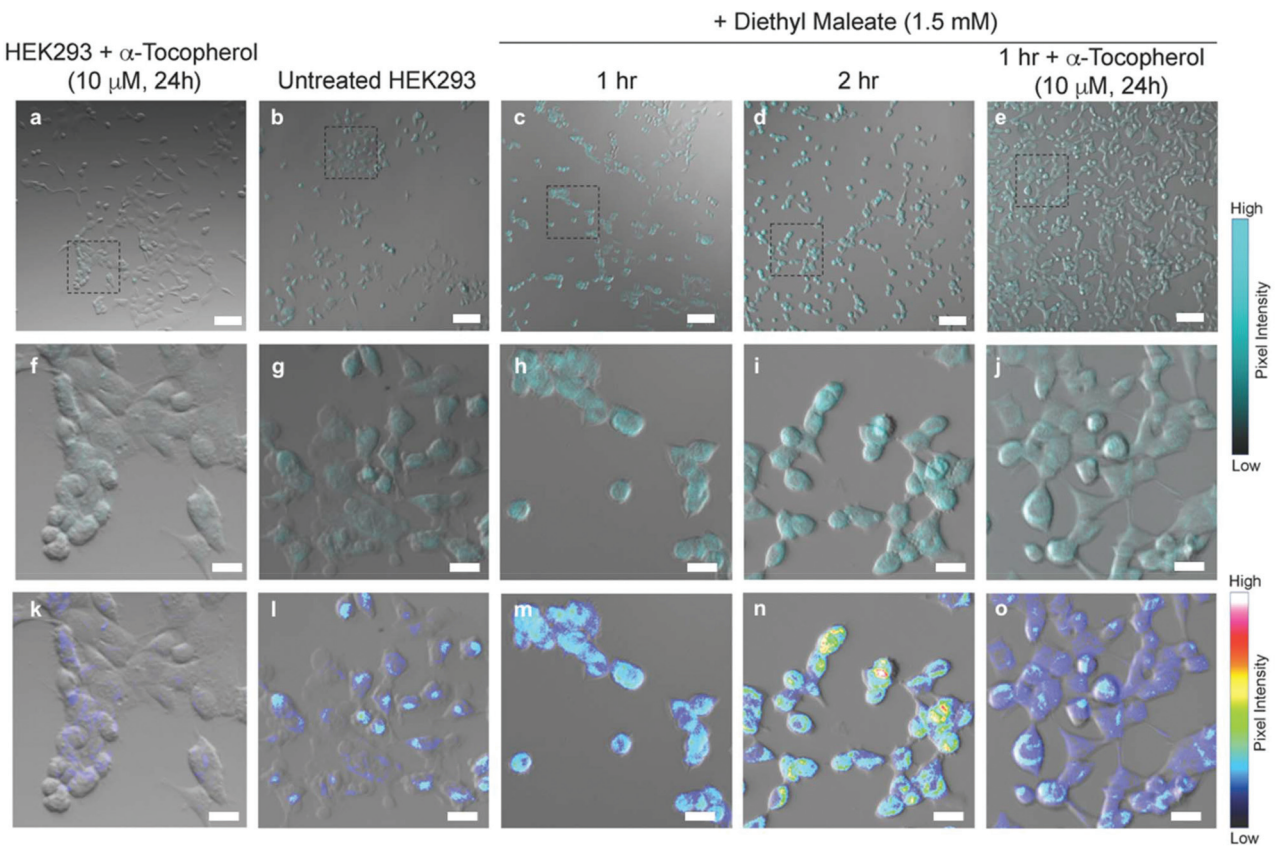

Fig. 8 Live cell microscopy of HEK293 cells incubated with diethyl maleate (DEM) to induce lipid peroxidation, and/or α-tocopherol (α-TOH) as an anti-oxidant. HEK293 cells were either left untreated (b, g, l), treated with 1.5 mM diethyl maleate for 1 h (c, h, m) or 2 h (d, i, n), or treated with α-tocopherol (10 mM, 24 h) (a, f, k) alone or prior to DEM (1.5 mM, 1 h) (e, j, o) and were then incubated with 100 μM **2b** for 5 min prior to imaging. The fluorescence micrographs overlayed on DIC images for the full field of view (top), as well as a zoom region (middle) are shown. Zoom region is indicated by black dashed boxes. Heat map overlay of the fluorescence intensity shows relative distribution of imaging signal intensity in HEK293 cells (bottom). Scale bars for panels a–e = 100 μm, and panels f–o = 25 μm. All images were acquired with 405 nm excitation laser, and an emission window of 420 to 520 nm.

after 1 h of DEM treatment in some cells, which continues to increase in both intensity and frequency after 2 h of incubation. In order to reduce aldehydic load, HEK293 cells were treated with 10 μM α-TOH for 24 h and left untreated (Fig. 8a, f and k) or treated with 1.5 mM DEM for 1 h (Fig. 8e, j and o) prior to incubation with **2b** for 5 min. A reduction of aldehydic load was observed following both treatments, with α-TOH reducing DEM-induced aldehyde production, as well as homeostatic aldehyde production in the cultured cells. Although the specific identity of the aldehydes contributing to the fluorescence enhancement observed in HEK293 cells cannot be determined using **2b**, the broad reactivity of the probe for aliphatic aldehydes in general provides a good measure of Aldehydic Load, an important emerging biomarker for studying a range of diseases.[30]

Conclusions

The use of methyl 5-MeO-*N*-aminoanthranilate dihydrochloride (**2b**) as a fluorogenic probe capable of detecting endogenous aldehydes was examined in detail. The current work complements a previous description of **2b** in the context of fluorescent fingerprinting of aldehydes,[12] and seeks to fully describe its intra- and intermolecular reactivity, as well as the utility of **2b** for live cell microscopy of aldehydic load. The reaction of **2b** with MDA (formed *in situ* from MDA tetramethyl acetal) was found to produce a blue fluorescent pyrazole **4b** (λ_{em} 410 nm, Φ 0.45), proceeding through a blue-green fluorescent hydrazone intermediate **10**. The simple structures of both **2b** and **4b** facilitated a detailed ^{1}H NMR-based mechanistic evaluation of the reaction, presenting evidence of the hydrazone intermediate that was also supported by fluorescence spectroscopy studies. The selectivity of **2b** toward the detection of cellular components was also evaluated, revealing that in addition to MDA, a significant fluorogenic response is observed with simple aliphatic aldehydes. Longer chain aliphatic aldehydes, produced, for example, during lung cancer progression, led to the formation of fluorescent hydrazones (**3f–3i**), emitting in the "far" blue region (λ_{em} 466–480 nm). Quantum yields associated with these fluorophores were found to be modest (Φ 0.06–0.17), attributable to the occurrence of hydrazones as inseparable mixtures of *E*- and *Z*-isomers. One caveat for the use of **2b** for Aldehydic Load imaging derives from the instability of hydrazine **2b** in aqueous solution and the minute time-scale lifetime of the hydrazone intermediate **10**, limiting detection reliability to within 5 min of probe application. Even with this caveat in place, Aldehydic Load enhancement following oxidative stress-induced lipid peroxidation was successfully imaged through live cell microscopy of HEK293 cells treated with DEM. Overall our results present a detailed evaluation of the reaction between a fluorogenic hydrazine-derived probe and MDA, and might provide a useful guideline for the development of rapid and easy to perform fluorescence assays for point-of-care detection of Aldehydic Load relevant to a variety of diseases. The uniqueness of methyl 5-MeO-*N*-aminoanthranilate derives from its minimal nature: facile synthesis for easy accessibility, simple wash-free implementation for live cell microscopy, and broad aliphatic aldehyde binding for total aldehyde load mapping. In effect, the minimalism of the probe maximizes its application to evaluate the chemical biology of carbonyls. Future studies will involve chemical modifications of **2b** to prevent the spontaneous cyclization in PBS, the formation of fluorescent molecules emitting at longer wavelengths (λ_{em} > 500 nm), and the application of **2b** to interrogate the chemical biology of endogenous aldehydes in cellular models of disease.

Experimental

General experimental procedures

Reagents were commercially available, except for 5-MeO-*N*-aminoanthranilic acid (**2a**),[5b] methyl 5-MeO-*N*-aminoanthranilate dihydrochloride (**2b**),[12] pyrazoles **4a**, **4b**[12] and indazole **11**[25] which were prepared according to the literature procedures. All solvents were HPLC grade except for water (18.2 MΩ cm millipore water). Solvents were removed under reduced pressure in a rotary evaporator, aqueous solutions were lyophilized and organic extracts were dried over Na_2SO_4. Flash column chromatography (FCC) was carried out using silica gel (SiO_2), mesh size 230–400 Å. Thin-layer chromatography (TLC) was carried out on Al backed silica gel plates with compounds visualised by anisaldehyde stain, 5% ninhydrin stain, and UV light. NMR spectra were recorded on a 300 or 400 MHz spectrometers, for ^{1}H NMR spectra δ values were recorded as follows: DMSO-D_6 (2.50 ppm); for ^{13}C (93.75 or 125 MHz) δ DMSO-D_6 (39.50 ppm). Mass spectra (MS) were obtained using electron impact (EI). Steady state fluorescence spectra were acquired on a Cary Eclipse fluorescence spectrophotometer, using 1× PBS, pH 7.2 containing up to 10% DMSO. Quantum yields were determined as described previously,[31] using harmane as a standard.[13]

Reaction of 2b with aliphatic aldehydes (pentanal, hexanal, octanal, nonanal)

Aliphatic aldehydes (pentanal, 53 μL; hexanal, 61 μL; octanal, 78 μL; nonanal, 86 μL; 0.5 mmol each) were added to separated stirred solutions of methyl 5-MeO-*N*-aminoanthranilate dihydrochloride (**2b**, 132 mg, 0.5 mmol) in MeOH (5 mL) and water (1.25 mL). The mixtures were stirred for 18 h at rt; MeOH was evaporated, the residues were diluted with brine (30 mL) and were extracted with EtOAc (2 × 30 mL). Combined organic extracts were dried, were concentrated and the residues were subjected to FCC on 40 g SiO_2 as follows: hydrazone **3f**, hexanes/EtOAc (4 : 1); hydrazones **3g–3i**, hexanes/EtOAc (9 : 1). Evaporation of the eluates afforded hydrazones **3f–3i**.

Hydrazone 3f. Yellow oil, mixture of *E*- and *Z*-isomers, 110 mg, 83%. ^{1}H NMR δ (DMSO-D_6) 10.51 (s, D_2O exch., 0.4H); 10.33 (s, D_2O exch., 0.6H); 7.53 (d, J = 9.0 Hz, 0.4H); 7.43 (d, J = 9.0 Hz, 0.6H); 7.37 (t, J = 5.0 Hz, 0.6H); 7.32 (d, J = 3.0 Hz, 0.4H); 7.27 (d, J = 3.0 Hz, 0.6H); 7.18 (dd, J = 9.0, 3.0 Hz, 0.4H); 7.14 (dd, J = 9.0, 3.0 Hz, 0.6H); 6.59 (t, J = 5.0 Hz, 0.4H); 3.86

(s, 1.2H); 3.83 (s, 1.8H); 3.72 (s, 1.2H); 3.71 (s, 1.8H); 2.23 (m, 2H); 1.45 (m, 4H); 0.90 (m, 3H). ^{13}C NMR δ (DMSO-D_6) 167.9, 167.4, 150.9, 150.4, 144.2, 142.8, 142.4, 142.3, 123.2 (2 × C), 114.8, 114.7, 112.6 (2 × C), 108.8, 108.1, 55.4 (2 × C), 52.2, 51.9, 31.5, 28.5, 27.5, 26.1, 22.0, 21.7, 13.8, 13.7. HRMS (EI) *m*/*z*; found 264.1473 [M+] (calcd 264.1474 for $C_{14}H_{20}N_2O_3$), LRMS (EI) *m*/*z* (rel. abundance): 264 [M+] (100), 180 (87), 164 (24), 150 (49), 122 (53).

Hydrazone 3g. Yellow oil, mixture of *E*- and *Z*-isomers, 85 mg, 61%. ^{1}H NMR δ (DMSO-D_6) 10.51 (s, D_2O exch., 0.4H); 10.33 (s, D_2O exch., 0.6H); 7.53 (d, J = 9.0 Hz, 0.4H); 7.47 (d, J = 9.0 Hz, 0.6H); 7.37 (t, J = 5.0 Hz, 0.6H); 7.32 (d, J = 3.0 Hz, 0.4H); 7.27 (d, J = 3.0 Hz, 0.6H); 7.18 (dd, J = 9.0, 3.0 Hz, 0.4H); 7.14 (dd, J = 9.0, 3.0 Hz, 0.6H); 6.58 (t, J = 5.0 Hz, 0.4H); 3.86 (s, 1.2H); 3.83 (s, 1.8H); 3.72 (s, 1.2H); 3.71 (s, 1.8H); 2.22 (m, 2H); 1.53 (m, 2H); 1.33 (m, 4H); 0.89 (m, 3H). ^{13}C NMR δ (DMSO-D_6) 167.9, 167.4, 150.9, 150.4, 144.2, 142.8, 142.4, 142.3, 123.2, 123.1, 114.8, 114.7, 112.7, 112.6, 108.8, 108.2, 55.4 (2 × C), 52.2, 51.9, 31.7, 31.0, 30.8, 26.3, 26.0, 25.0, 21.9, 21.8, 13.9, 13.8. HRMS (EI) *m*/*z*; found 278.1638 [M+] (calcd 278.1630 for $C_{15}H_{22}N_2O_3$), LRMS (EI) *m*/*z* (rel. abundance): 278 [M+] (100), 180 (83), 164 (43), 150 (37), 122 (38).

Hydrazone 3h. Yellow oil, mixture of *E*- and *Z*-isomers, 119 mg, 78%. ^{1}H NMR δ (DMSO-D_6) 10.51 (s, D_2O exch., 0.4H); 10.32 (s, D_2O exch., 0.6H); 7.53 (d, J = 9.0 Hz, 0.4H); 7.47 (d, J = 9.0 Hz, 0.6H); 7.37 (t, J = 5.0 Hz, 0.6H); 7.32 (d, J = 3.0 Hz, 0.4H); 7.28 (d, J = 3.0 Hz, 0.6H); 7.18 (dd, J = 9.0, 3.0 Hz, 0.4H); 7.14 (dd, J = 9.0, 3.0 Hz, 0.6H); 6.59 (t, J = 5.0 Hz, 0.4H); 3.86 (s, 1.2H); 3.83 (s, 1.8H); 3.72 (s, 1.2H); 3.71 (s, 1.8H); 2.23 (m, 2H); 1.53 (m, 2H); 1.32 (m, 8H); 0.85 (m, 3H). ^{13}C NMR δ (DMSO-D_6) 167.9, 167.4, 150.9, 150.4, 144.2, 142.8, 142.4, 142.3, 123.2, 123.1, 114.8, 114.6, 112.6 (2 × C), 108.8, 108.1, 55.4 (2 × C), 52.1, 51.9, 31.8, 31.2, 31.1, 28.8, 28.6, 28.5, 28.4, 26.4, 26.3, 25.4, 22.1 (2 × C), 13.9 (2 × C). HRMS (EI) *m*/*z*; found 306.1953 [M+] (calcd 306.1943 for $C_{17}H_{26}N_2O_3$), LRMS (EI) *m*/*z* (rel. abundance): 306 [M+] (100), 180 (79), 164 (34), 150 (36), 122 (40).

Hydrazone 3i. Yellow oil, mixture of *E*- and *Z*-isomers, 119 mg, 74%. ^{1}H NMR δ (DMSO-D_6) 10.51 (s, D_2O exch., 0.4H); 10.32 (s, D_2O exch., 0.6H); 7.52 (d, J = 9.0 Hz, 0.6H); 7.47 (d, J = 9.0 Hz, 0.4H); 7.37 (t, J = 5.5 Hz, 0.4H); 7.32 (d, J = 3.0 Hz, 0.6H); 7.27 (d, J = 3.0 Hz, 0.6H); 7.18 (dd, J = 9.0, 3.0 Hz, 0.6H); 7.14 (dd, J = 9.0, 3.0 Hz, 0.4H); 6.59 (t, J = 5.5 Hz, 0.6H); 3.86 (s, 1.8H); 3.83 (s, 1.2H); 3.72 (s, 1.8H); 3.70 (s, 1.2H); 2.22 (m, 2H); 1.53 (m, 2H); 1.36 (m, 10H); 0.85 (m, 3H). ^{13}C NMR δ (DMSO-D_6) 167.9, 167.4, 151.0, 150.5, 144.2, 142.8, 142.4 (2 × C), 123.2, 123.1, 114.8, 114.7, 112.7, 112.6, 108.8, 108.2, 55.4 (2 × C), 52.1, 51.9, 31.8, 31.3, 31.2, 28.9, 28.8, 28.7, 28.6 (3 × C), 26.4, 26.3, 25.4, 22.1 (2 × C), 13.9 (2 × C). HRMS (EI) *m*/*z*; found 320.2081 [M+] (calcd 320.2100 for $C_{18}H_{28}N_2O_3$), LRMS (EI) *m*/*z* (rel. abundance): 320 [M+] (32), 180 (52), 164 (19), 150 (22), 122 (21).

Reaction of 2a and 2b with MDA – detailed kinetic analysis

NMR study. Separate solutions of **2a** or **2b** (1 mg each) in 1× PBS, pH 7.2 containing 10% DMSO-D_6 were prepared and the ^{1}H NMR spectra were acquired. The tubes were then removed from the spectrometer, 1 drop of 1 M solution of MDA tetramethyl acetal in 1 M HCl (known to form MDA *in situ*)[24] was added and ^{1}H NMR spectra were acquired immediately (1 min) and then after 2, 4, 20 and 120 (**2b** only) minutes. Separate solutions of pyrazoles **4a**, **4b** and MDA (controls) were prepared and analyzed under identical conditions.

Fluorescence study. A 10 mM stock solution of **2b** was prepared in DMSO, and 5 μL was added to 1× PBS, pH 7.2, in a 1 cm path length quartz cuvettes, followed by mixing by inversion. To this solution, 50 μL of 1 M solution of MDA tetramethyl acetal in 1 M HCl was added,[24] immediately followed by 5 μL of 10 M NaOH to neutralize the solution (as confirmed by a pH paper). Fluorescence emission was recorded on a fluorescence spectrophotometer with $\lambda_{ex}/\lambda_{em}$ 310/410 nm and 375/475 nm and slit widths of 5 nm. Readings were acquired concurrently every 10 s for 45 min, the experiment was repeated three separate times.

Hydrazine 2b as a fluorogenic probe for Aldehydic Load

Detection of MDA. The samples were prepared as follows: 100 μL of the solution of **2b** (10^{-5} M) in DMSO was mixed with 1× PBS (pH 7.2) and a stock solution of MDA[24] was added to achieve the final volume of 1 mL (final concentration of **2b** in the sample is 10^{-6} M). Seven separate samples were prepared, the concentrations of MDA were 10^{-7} M (0.1 eq.), 2×10^{-7} M (0.2 eq.), 5×10^{-7} M (0.5 eq.), 10^{-6} M (1 eq.), 2×10^{-6} M (2 eq.), 5×10^{-6} M (5 eq.), 8.5×10^{-6} M (8.5 eq.). The pH in the samples containing larger amounts of MDA stock solution (>2 eq.) was adjusted (to reach ~pH 7.2) by the addition of saturated $NaHCO_3$ solution (10–20 μL). Control samples containing just hydrazine **2b**, pyrazole **4b** and MDA (final concentration of 10^{-6} M) were also prepared. Each sample was analyzed right after preparation (within 1 min) by fluorescence scans (λ_{ex} 371 nm or 307 nm). All measurements were performed at 37 °C. The same temperature was maintained to keep the MDA stock solution as well as PBS. The stock solution of hydrazine **2b** in DMSO was stored at rt in the dark (flask wrapped in Al foil). Bell-type curves were fitted to raw data points of emission scans using standard protocols in GraphPad Prism v.7.0c.

Response to other carbonyls, metal ions and biologically relevant molecules. The samples containing **2b** (final concentration 10^{-6} M) were prepared as described above. A solution of 5 eq. of the analyte of interest was added (final concentration 5×10^{-6} M), the fluorescence scans (λ_{ex} 371 nm) were performed as described above.

Instability of 2b in PBS. A solution of hydrazine **2b** in DMSO (100 μL) was mixed with PBS (overall volume 1 mL, final concentration 10^{-6} M, 37 °C). The fluorescence scans (λ_{ex} 327 nm) were performed immediately (1 min), then after 5 and 20 min. A sample containing indazole **11** was prepared and analyzed under identical conditions.

Live-cell microscopy study. HEK293 cells were a gift from the lab of Dr D. A. Pratt (University of Ottawa). Cells were cultured in Minimal Essential Medium supplemented with 10% v/v Fetal Calf Serum, 1% v/v Pen Strep antibiotic solution, and 1%

MEM non-essential amino acid solution at 37 °C in a 5% CO_2 atmosphere. Cells were plated at 25 000 cells per well in a 24-well tissue culture-treated polystyrene plate overnight prior to use for microscopy. Growth medium was changed prior to treatment with 10 μM α-TOH for 24 h, or 1.5 mM DEM for 1 and 2 h. At indicated time points, media was removed and replaced with 1× Hank's Balanced Salt Solution, pH 7.2, and 10 μL of a solution of **2b** in DMSO (final concentration of **2b** = 100 μM) was added. Imaging was performed on a Zeiss LSM 880 confocal microscope fitted with live cell incubator chamber using 405 nm excitation laser line, and 10x objective lens. Both, differential interference contrast (DIC) and fluorescence images were acquired. All image analysis was performed using ImageJ v1.45S.

Conflicts of interest

The authors declare no competing financial interest.

Acknowledgements

We wish to acknowledge Professor Jeffrey Keillor for allowing us to use his Cary Eclipse Fluorescence Spectrophotometer for the duration of this work. This work was supported by an NSERC Discovery Grant RGPIN 2015-05796 (A. J. S.), the Canada Research Chairs Program 950-230754 (A. J. S.), and the Canadian Institutes of Health Research PJT376892 (A. J. S.); the financial support provided by these agencies is gratefully acknowledged.

Notes and references

1 O. K. Abou-Zied, B. Y. Al-Busaidi and J. Husband, *J. Phys. Chem. A*, 2014, **118**, 103.
2 According to a recent review, fluorescence properties associated with anthranilates have never been integrated into imaging probe development see: (*a*) R. Duval and C. Duplais, *Nat. Prod. Rep.*, 2017, **34**, 161. For an isolated example exploiting the blue fluorescence of anthranilic acid within the context of chemical biology see: (*b*) C. Coburn, E. Allman, P. Mahanti, A. Benedetto, F. Cabreiro, Z. Pincus, F. Mathijssens, C. Araiz, A. Mandel, M. Vlachos, S. A. Edwards, G. Fischer, A. Davidson, R. E. Pryor, A. Stevens, F. J. Sack, N. Tavernarakis, B. P. Braeckman, F. C. Schroeder, K. Nehrke and D. Gems, *PLoS Biol.*, 2013, **11**, e1001613.
3 While the functionalization of anthranilic acids to form anthranilamides is well developed, see.(*a*) N. Kanişkan, Ş. Kökten and İ. Çelik, *ARKIVOC*, 2012, **viii**, 198 and references cited therein, the modification of the benzene ring to allow for the conjugation of anthranilic acids by *e.g.* "click" reaction is underdeveloped. For an isolated example see: (*b*) C. S. McKay and M. G. Finn, *Angew. Chem., Int. Ed.*, 2016, **55**, 12643.
4 (*a*) P. Crisalli and E. T. Kool, *Org. Lett.*, 2013, **15**, 1646; (*b*) P. Crisalli and E. T. Kool, *J. Org. Chem.*, 2013, **78**, 1184.
5 (*a*) E. T. Kool, D. H. Park and P. Crisalli, *J. Am. Chem. Soc.*, 2013, **135**, 17663; (*b*) T. Dang, M. Suchý, Y. J. Truong, W. Oakden, W. W. Lam, C. Lazurko, G. Facey, G. J. Stanisz and A. J. Shuhendler, *Chem. – Eur. J.*, 2018, **24**, 9148.
6 P. J. O'Brien, A. G. Siraki and N. Shangari, *Crit. Rev. Toxicol.*, 2005, **35**, 609.
7 O. E. Owen, V. E. Trapp, C. L. Skutches, M. A. Mozzoli, R. D. Hoeldtke, G. Boden and G. A. Reichard Jr., *Diabetes*, 1982, **31**, 242.
8 P. Fuchs, C. Loeseken, J. K. Schubert and W. Miekisch, *Int. J. Cancer*, 2010, **126**, 2663.
9 D. T. Antoniak, M. J. Duryee, T. R. Mikuls, G. M. Thiele and D. R. Anderson, *Free Radicals Biol. Med.*, 2015, **89**, 409.
10 S. Ivanova, G. I. Botchkina, Y. Al-Abed, M. Meistrell III, F. Batliwalla, J. M. Dubinsky, C. Iadecola, H. Wang, P. K. Gregersen, J. W. Eaton and K. J. Tracey, *J. Exp. Med.*, 1998, **188**, 327.
11 For selected examples see; (*a*) T. F. Brewer and C. J. Chang, *J. Am. Chem. Soc.*, 2015, **137**, 10886; (*b*) L. H. Yuen, N. S. Saxena, H. S. Park, K. Weinberg and E. T. Kool, *ACS Chem. Biol.*, 2016, **11**, 2312; (*c*) T. F. Brewer, G. Burgos-Barragan, N. Wit, K. J. Patel and C. J. Chang, *Chem. Sci.*, 2017, **8**, 4073; (*d*) K. J. Bruemmer, O. Green, T. A. Su, D. Shabat and C. J. Chang, *Angew. Chem., Int. Ed.*, 2018, **57**, 7508; (*e*) M. Yang, J. Fan, J. Zhang, J. Du and X. Peng, *Chem. Sci.*, 2018, **9**, 6758.
12 C. Lazurko, I. Radonjic, M. Suchý, G. Liu, A. G. Rolland-Lagan and A. J. Shuhendler, *ChemBioChem*, 2018, DOI: 10.1002/cbic.201800427, in press.
13 A. Pardo, D. Reyman, J. M. L. Poyato and F. Medina, *J. Lumin.*, 1992, **51**, 269.
14 Z. A. M. Zielinski and D. A. Pratt, *J. Org. Chem.*, 2017, **82**, 2817.
15 MDA is known to form adducts with DNA rapidly, see for example in. (*a*) D. Pluskota-Karwatka, A. J. Pawlowicz, M. Bruszyńska, A. Greszkiewicz, R. Latajka and L. Kronberg, *Chem. Biodiversity*, 2010, **7**, 959; (*b*) K. Salus, M. Hoffmann, T. Siodla, B. Wyrzykiewicz and D. Pluskota-Karwatka, *New J. Chem.*, 2017, **41**, 2409.
16 A. Gönenç, Y. Ozkan, M. Torun and B. Simşek, *J. Clin. Pharm. Ther.*, 2001, **26**, 141.
17 M. Viigimaa, J. Abina, G. Zemtsovskaya, A. Tikhaze, G. Konovalova, E. Kumskova and V. Lankin, *Blood Press.*, 2010, **19**, 164.
18 L. S. Bir, S. Demir, S. Rota and M. Köseoğlu, *Tohoku J. Exp. Med.*, 2006, **208**, 33.
19 I. Hajimohammadreza and M. Brammer, *Neurosci. Lett.*, 1990, **112**, 333.
20 V. Nair and G. A. Turner, *Lipids*, 1984, **19**, 804.
21 D. R. Janero, *Free Radicals Biol. Med.*, 1990, **9**, 515.
22 J. Chen, L. Zeng, T. Xia, S. Li, T. Yan, S. Wu, G. Qiu and Z. Liu, *Anal. Chem.*, 2015, **87**, 8052.
23 L. He, X. Yang, K. Xu and W. Lin, *Chem. Commun.*, 2017, **53**, 4080.
24 Y. Tsuruta, Y. Date, H. Tonogaito, N. Sugihara, K. Furuno and K. Kohashi, *Analyst*, 1994, **119**, 1047.
25 L. Baiocchi, G. Corsi and G. Palazzo, *Synthesis*, 1978, 633.
26 F. Shahidi, *Adv. Exp. Med. Biol.*, 2001, **488**, 113.

27 M. Corradi, P. Pignatti, P. Manini, R. Andreoli, M. Goldoni, M. Poppa, G. Moscato, B. Balbi and A. Mutti, *Eur. Respir. J.*, 2004, **24**, 1011.
28 D. Poli, M. Goldoni, M. Corradi, O. Acampa, P. Carbognani, E. Internullo, A. Casalini and A. Mutti, *J. Chromatogr. B: Anal. Technol. Biomed. Life Sci.*, 2010, **878**, 2643.
29 B. Li, F. Zheng, J. R. Chauvin and D. A. Pratt, *Chem. Sci.*, 2015, **6**, 6165.
30 (*a*) L. H. Yuen, N. S. Saxena, H. S. Park, K. Weinberg and E. T. Kool, *ACS Chem. Biol.*, 2016, **11**, 2312; (*b*) E. M. Ellis, *Pharmacol. Ther.*, 2007, **115**, 13.
31 D. F. Eaton, *J. Photochem. Photobiol., B*, 1988, **2**, 523.